Chinese Journal of
POLYMER SCIENCE

RESEARCH ARTICLE

https://doi.org/10.1007/s10118-023-3058-4
Chinese J. Polym. Sci. **2024**, *42*, 344–351

Critical Role of Ethylene-Propylene Block Copolymer in Impact Polypropylene Copolymer

Yu-Hui Tang[a,b], Na Zhang[a,b], Wei Bao[a,b], Wei Jiang[a,b], Yuan Lin[a], and Zhao-Hui Su[a,b*]

[a] *State Key Laboratory of Polymer Physics and Chemistry, Changchun Institute of Applied Chemistry, Chinese Academy of Sciences, Changchun 130022, China*
[b] *School of Applied Chemistry and Engineering, University of Science and Technology of China, Hefei 230026, China*

Abstract Ethylene-propylene block copolymer (EbP) is a vital component in impact polypropylene copolymer (IPC), yet its distribution in the multiphase composite material and how it influences the phase structure and the mechanical properties are not well understood. In this work, four IPCs were investigated by atomic force microscopy-infrared (AFM-IR) to assess the phase compositions *in situ*, based on which in conjunction with the chain microstructure information obtained *ex situ* the distributions of the copolymer components were derived for each alloy. For the IPCs whose EbP comprises long P and long E segments, the EbP fraction was found to phase separate from the rubber and the PP matrix to form the cores of the disperse particles with the E-P segmented copolymer (EsP). In contrast, in the IPC with EbP composed of long P and short E segments, the EbP fraction formed an outer shell for the rubber particles with the cores comprising the EsP alone, and this IPC, containing a lower E comonomer content than its counterpart, exhibited both better impact resistance and higher flexural modulus. These results clarify how the chain structure of EbP governs the phase morphology in IPC, which in turn impacts the properties of the composite material.

Keywords Impact polypropylene copolymers; AFM-IR; Ethylene-propylene block copolymers; Core-shell rubber particles

Citation: Tang, Y. H.; Zhang, N.; Bao, W.; Jiang, W.; Lin, Y.; Su, Z. H. Critical role of ethylene-propylene block copolymer in impact polypropylene copolymer. *Chinese J. Polym. Sci.* **2024**, *42*, 344–351.

INTRODUCTION

Impact polypropylene copolymer (IPC) has been used extensively in automotive, packaging and other industries in recent years because of its many excellent properties, such as balanced rigidity and impact resistance at low temperatures, good processability and chemical stability. It is an alloy of PP produced in the reactor in two steps. First, propylene monomers are polymerized using a Ziegler-Natta (ZN) catalyst to generate isotactic PP, which provides stiffness for the end product, and then, a mixture of propylene and ethylene is introduced to make ethylene-propylene copolymers to toughen the material *in situ*.[1,2] The polymerization in the second step is complex, generating ethylene-propylene block copolymers (EbPs) with different block lengths and distributions,[3] ethylene-propylene random copolymer (EPR) and possibly a small amount of ethylene homopolymer in addition to PP homopolymer.[4,5] In the subsequent melt processing, these components undergo phase separation and phase reorganization, and form rubber particles with multilayer structure dispersing in the PP matrix.[6] The rubber particles are about several hundred nanometers to several microns in diameter, and their internal structure, dispersion in and interactions with the PP matrix together affords the IPC a good property balance between the stiffness and the toughness.[7–10]

Since the properties of IPC depend the complex composition and phase structure,[7,11,12] it has attracted much attention over the years. The different components in IPC have been extracted by temperature rising elution fractionation (TREF) and their chain structures determined,[13–18] based on which a model of multilayered rubber particles dispersed in PP matrix was proposed. In this well accepted model, the core of the particle comprises EbPs with long E blocks and PE homopolymer and thus is mainly crystalline PE, which is encapsulated by an amorphous and rubbery inner layer of EPR, with an outer shell between the rubber layer and the PP matrix consisting of PE and PP crystallites.[19] This model is further supported by the morphologies observed for IPC thin films cast from solution and corresponding selected area electron diffraction results.[20,21] While it is unambiguous that the EPR is responsible for improving the toughness of the composite material, the roles of the EbPs remain not well understood and have been the topic of much research. For example, Qiu *et al*. used the fractions isolated from a commercial IPC to prepare PP/EPR/EbP blends by solution-mixing[22] and found that the EbP served as a compatibilizer between the PP matrix and the EPR, affecting the interfacial area and the number and morphology of the dispersed particles. It was observed that when the EbP content decreased, there were fewer particles with the core-shell structure and more of single EPR rubber phase. Rungswang *et al*. studied the structure of crystallizable

* Corresponding author, E-mail: zhsu@ciac.ac.cn
Received July 13, 2023; Accepted October 9, 2023; Published online November 10, 2023

EbP in IPCs with different mechanical properties, and inferred that EbPs with high contents of long P segments might co-crystalize with the PP matrix, which helped increasing the rigidity.[23] Tan *et al*. observed higher toughness in IPC upon increasing the content of crystallizable EbP in the system, and attributed the effects to improved compatibility between the EPR disperse phase and the PP matrix with the crystallizable EbP acting as the compatibilizer.[4] However, the studies in the literature so far have based on analyses of fractions isolated from IPC materials and the phase structure rebuilt by solution blending of these fractions, whereas experimental evidence obtained *in situ* on the roles that EbP plays is lacking.

Atomic force microscopy-infrared (AFM-IR) is a technique emerging in recent years enabling spectroscopic analysis at a sub-100 nm spatial resolution, and has been employed in investigation of nanoscopic domains *in situ* in polymeric systems.[24–26] By using this powerful technique, our group established a quantitative method to analyze *in situ* the compositions of nanoscopic domains in IPC,[27] and found that in some commercial IPCs the rigid cores of the rubber particles are dominated by PP rather than PE as predicted by the established model,[28] which indeed is beneficial to the stiffness of the alloy.[10,29]

The aim of the present study is to elucidate the effects of EbP on the phase structure formation and mechanical properties of IPC. Two sets of commercial IPCs are investigated. In the first set we compare two alloys of similar chain structure for each fraction and hence similar phase structure, and show that the one with a higher ethylene content has better impact strength as expected. In contrast, the two IPCs in the second set exhibit different phase structure, and the one containing less ethylene units is indeed more impact resistant and stiffer, and we show that the EbP fraction is responsible for these effects. Our findings are reported herein.

EXPERIMENTAL

Materials

Four commercial IPC resins collected from the market were used in this study, the basic information of which is listed in Table 1.

Characterization

Melt flow rates (MFRs) were measured on a melt indexer (XNR-400C, Chengde Jinhe Instrument Manufacturing Co., Ltd., China) under the load of 2.16 kg at 230 °C. Notched Izod impact was performed on a tester (XJU-2.75, Chengde Testing Machine Factory, China) following GB/T1843-2008 standard. The test specimens were of 63.5 mm × 12.7 mm × 3.2 mm (length × width × thickness) in size, with a 45° V-shaped notch (2.5 mm depth), and were maintained at the designated temperature (23±2 or −30±2 °C) for 24 h before testing. Flexural strength was measured at room temperature (23±2 °C) by using a universal testing machine (Instron-1121, UK) at 2 mm/min according to GB/T 9341-2008 standard. The dimensions of the specimens were 80 mm × 10 mm × 4 mm (length × width × thickness). The result for each sample was an average of five replicates.

FTIR spectra were recorded on a ThermoNicolet 6700 spectrometer equipped with a MCT detector using the attenuated total reflectance mode (ZnSe crystal, 45°, Pike Technologies) at 4 cm^{-1} resolution. The samples were hot pressed into thin films for testing.

Differential scanning calorimetric (DSC) thermograms were collected on a DSC Q20 calorimeter (TA Instruments) under nitrogen atmosphere. The sample (5–10 mg) was first heated to 200 °C at a rate of 100 °C/min and held at that temperature for 5 min to erase the thermal history. Then, the sample was cooled down to 20 °C, maintained for 1 min and then heated to 200 °C at a ramping rate of 10 °C/min. The crystallization temperature (T_c) and the melting temperature (T_m) was obtained from the cooling and the reheating run, respectively.

Wide-angle X-ray diffraction (WAXD) patterns were recorded with a semiconductor detector with a resolution of 487 × 195 (pixel size=172 μm) (Pilatus100K, Dectris, Swiss) connected to a multilayer mirror (FOX3D 21-21, Xenocs SA, France) with a focused Cu K_α X-ray source (0.154 nm wavelength, Genix3D Xenocs SA, France) operating at 50 kV and 0.6 mA. Fit2D software was used for background comparison and data analysis.

AFM-IR analyses were carried out on a first generation nanoIR™ (Anasys Instruments). The samples were sliced into thin films of 200–400 nm thickness by cryomicrotomy at −120 °C, which were placed on a ZnSe prism mounted on the instrument. AFM images were acquired in contact mode using an EX-C450 tip, and then the sample was illuminated from underneath in a total internal reflection mode by an Ekspla optical parametric oscillator laser with a tuning range of 900–2000 cm^{-1} and a spectral resolution of 4 cm^{-1}, and AFM-IR spectrum was generated by measuring with the AFM tip the thermal expansion of the sample as a function of the laser wavelength normalized by the laser intensity averaged over 128 pulses.

RESULTS AND DISCUSSION

Four commercial IPC samples are selected and investigated in this study. Their FTIR spectra in the 1550–650 cm^{-1} region are displayed in Fig. 1. The four spectra are almost identical, dominated by the symmetric CH_3 bending at 1378 cm^{-1}, the CH_2 bending and asymmetric CH_3 deformation at 1456 cm^{-1},[30,31] with other PP characteristic bands at 1167, 998, 973, 900, 841 and 809 cm^{-1}, as well as the methylene rocking band at ~720 cm^{-1} due to long ethylene sequences, consistent with that re-

Table 1 Characteristics of the four IPCs.

Sample	Ethylene content (wt%)	MFR (g/10min)	Flexural modulus (MPa)	Notched izod impact strength (kJ/m^2)	
				23 °C	−30 °C
IPC-1	15.98	45.5	951.7±32.1	3.87±0.25	3.19±0.29
IPC-2	10.23	49.2	955.6±28.5	2.90±0.14	2.47±0.40
IPC-3	9.13	61.0	1498.4±38.6	2.52±0.14	1.95±0.11
IPC-4	6.04	54.6	1828.0±69.4	3.86±0.22	2.18±0.21

https://doi.org/10.1007/s10118-023-3058-4

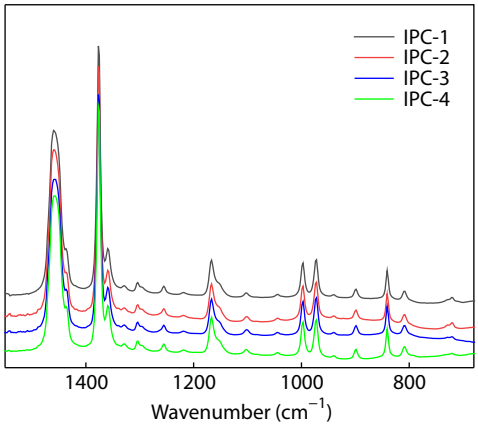

Fig. 1 FTIR spectra of the four IPCs.

ported for typical IPCs.[30,32,33] Table 1 lists the basic characteristics of these four IPCs. The first two are of medium flow, and the one with a higher ethylene content (IPC-1) is more impact resistant, as expected. Between the other two grades (high flow), however, the alloy containing less ethylene (IPC-4) is superior to the other in both impact resistance and stiffness, exhibiting the opposite trend. In-depth analyses are needed in order to identify the structural characteristics responsible for this unusual behavior.

Fig. 2 compares DSC heating traces of the four alloys in two groups. We see in Fig. 2(a) that the DSC curves for IPC-1 and IPC-2 are almost identical, dominated by the melting of crystalline PP at ~165 °C, with a weak melting peak observed at ~118 °C, signaling presence of crystallizable E segments in both alloys. For the two IPCs in the second group (Fig. 2b), significant difference is observed in their thermal properties. The weak melting peak at ~118 °C due to PE crystallites is observed for IPC-3, whereas it is absent in the heating curve of IPC-4, implying the lack of long and crystallizable ethylene sequences in the latter. Furthermore, the melting peak of the crystalline PP in IPC-4 is located at 168 °C, significantly higher than that for IPC-3, which suggests that the PP homopolymer in IPC-4 has a higher isotacticity, which is beneficial to the stiffness of the material.

The crystalline structures of the IPCs were assessed by WAXD as depicted in Fig. 3. The diffraction peaks characteristic of *α*-form crystals of isotactic PP at 14.0° (110), 17.0° (040), 18.6° (130), 21.0° (111), and 21.5° (131 and 041)[34] are observed for all four samples. In Fig. 3(a), the diffraction profiles for IPC-1 and IPC-2 are very similar, in line with the FTIR and DSC results. Moreover, the (040) and (130) diffractions of crystalline PP at 17.0° and 18.6° respectively for IPC-4 are stronger than that for IPC-3, implying more ordered PP crystalline structure in IPC-4, which contributes to its higher stiffness than the latter.

The four alloys have been fractionated by TREF and the molecular structure and compositions of the original resins and their fractions analyzed in great detail in a separate report.[35] It should be mentioned that the block copolymers generally are eluted as two distinct fractions. The fraction eluted at a lower temperature comprises short E and P segments and is named ethylene-propylene segmented copolymer (EsP), whereas the other one eluted at a higher temperature contains chains with E and P units in long sequences and is still called EbP.[3,36] The characteristics of the copolymer fractions of the four IPCs are listed in Table 2. By comparing the corresponding fractions, it can be seen that the chain structures of IPC-1 and IPC-2 are very similar, in particular the two EbP fractions contain roughly the same amount of E units, and the corresponding E and P block lengths are similar between the two segments. In contrast, significant difference exists in EbP between IPC-3 and IPC-4, the former comprising very long P and E blocks and the latter medium and short ones. How the chain structure affects the morphology, which subsequently impacts the physical properties of the IPC is the focus of this work, to be discussed later.

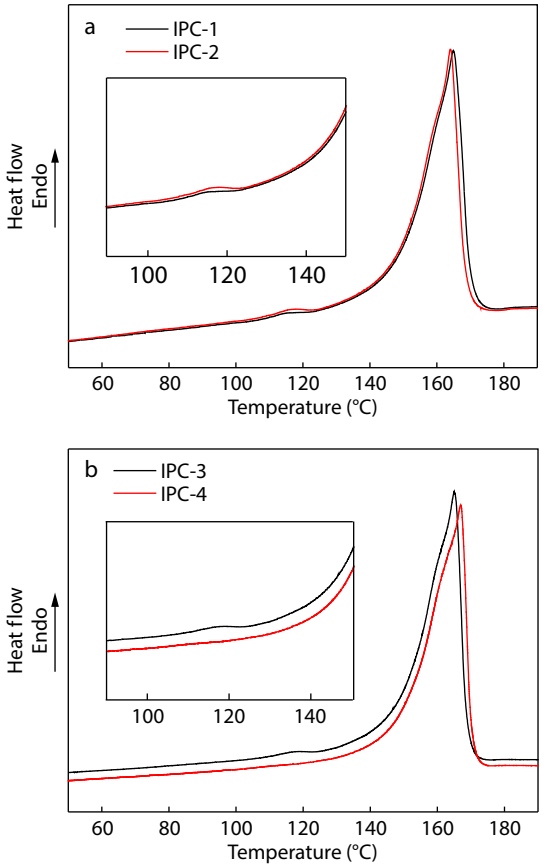

Fig. 2 DSC heating curves of the four IPCs.

Fig. 4 presents the morphology of the four alloys as examined by AFM, and the images show rubber particles with core-shell structure dispersed in the PP matrix in all cases, consistent with that of typical IPCs. In all these images the particles exhibit a broad size distribution, but we still can see that the particles in IPC-1 and IPC-2 roughly are of similar size (Figs. 4a and 4b), whereas for the second group, the difference in morphology between the two samples is obvious, with the dispersed particles in IPC-4 significantly smaller than that in IPC-3 (Figs. 4c and 4d).

Table 3 summarizes the size and volume fraction of the rubber particles in the four IPCs extracted from AFM images acquired. The volume fraction of the dispersed particles in IPC-1 and IPC-4 is 19.2% and 12.3%, respectively, with that for the other two in between, in line with the contents of EPR

https://doi.org/10.1007/s10118-023-3058-4

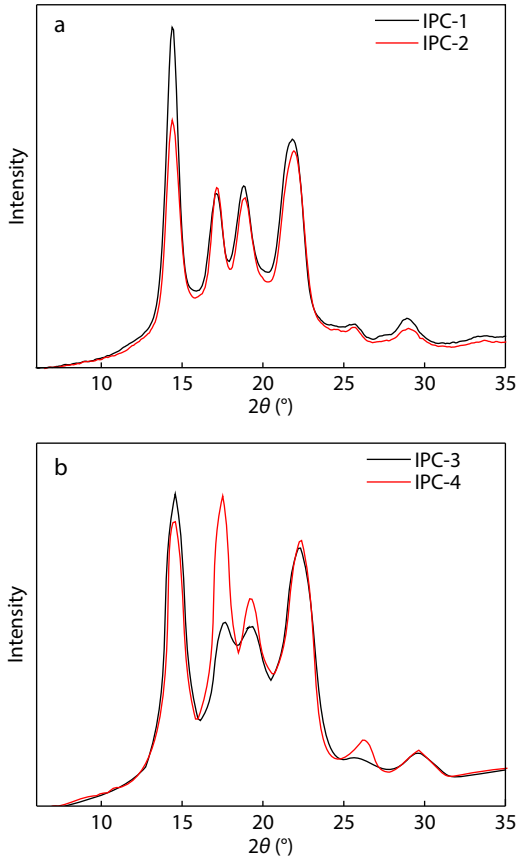

Fig. 3 WAXD profiles of the four IPCs.

Table 2 Characteristics of different fractions of the four IPCs.[35]

Sample	Fraction	Content (wt%)	Ethylene content (wt%)	Average segment length	
				n_P	n_E
IPC-1	EPR	18.05	45.70	2.0	2.6
	EsP	4.15	46.51	8.9	11.6
	EbP	4.04	16.92	119.0	36.4
IPC-2	EPR	16.18	40.48	2.5	2.5
	EsP	6.47	36.31	15.9	13.5
	EbP	6.66	15.98	152.9	43.5
IPC-3	EPR	12.71	37.15	2.7	2.4
	EsP	5.55	25.65	22.0	11.3
	EbP	6.23	10.01	668.5	112.0
IPC-4	EPR	11.00	36.03	2.6	2.2
	EsP	2.23	19.94	13.6	5.1
	EbP	2.63	8.62	51.7	7.5

fraction in these alloys revealed by TREF (Table 2). The size of rubber particles is known to affect the brittle-ductile transition of IPC, in particular the larger particles influence the impact behavior adversely.[37] The average diameter of the dispersed particle in IPC-1 and IPC-2 is about 0.63 and 0.64 μm, respectively, almost the same. In the second group, the rubber particles in IPC-3 are about 0.48 μm on average, whereas that in IPC-4 are much smaller, with an average diameter of 0.31 μm. The reason for this difference in dispersed particle size between IPC-3 and IPC-4 will become clear when the structures are better analyzed in following section.

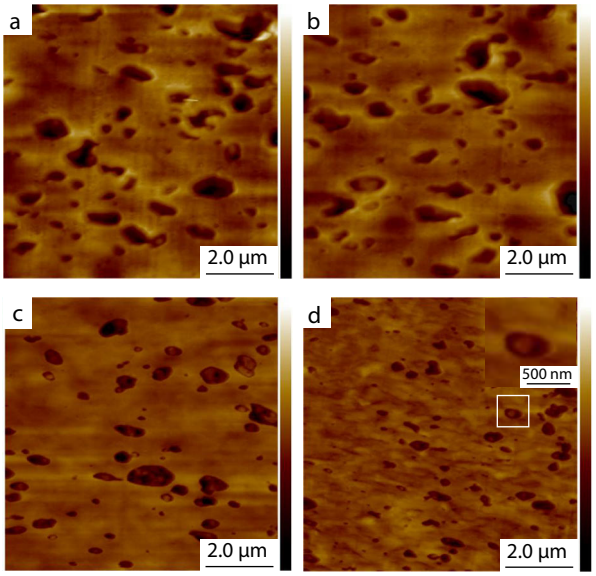

Fig. 4 AFM images of (a) IPC-1, (b) IPC-2, (c) IPC-3 and (d) IPC-4 (inset shows a core-shell particle in higher magnification).

Table 3 Size and volume fractions of the dispersed particles in the four IPCs.

Sample	Average diameter (μm)	Volume fraction (%)
IPC-1	0.63±0.33	19.2±2.6
IPC-2	0.64±0.33	15.5±3.4
IPC-3	0.48±0.28	14.6±2.6
IPC-4	0.31±0.22	12.3±1.8

Next, the composition of the different phases in the IPCs is analyzed *in situ* quantitatively by AFM-IR using a method established previously.[27,28] Fig. 5 displays typical AFM images of the IPC samples, each showing a core-shell rubber particle dispersed in PP matrix, and corresponding AFM-IR spectra in the 1500–1300 cm^{-1} region acquired for the core, rubber, and matrix domains, respectively, at the marked locations. The spectra are normalized to the methyl bending band at 1378 cm^{-1} in order to eliminate the effect of sample thickness, so that the ethylene contents in the three phases of the IPC can be better represented by the intensities of the 1456 cm^{-1} band. For the particular cases shown in Fig. 5, the spectra indicate that the ethylene content in the core is lower than that in the rubber phase. Multiple particles were thus analyzed for each IPC and the ethylene contents in the different phases derived quantitatively, which are listed in Table 4.

For all the four IPCs, the ethylene content in the matrix phase thus determined is essentially zero, in line with the fact that the matrix phase is PP homopolymer, validating the quantitative AFM-IR method. Moreover, for each alloy, the amount of ethylene in the rubber phase detected *in situ* by AFM-IR well matches that for the EPR fraction extracted from the same alloy determined by ^{13}C-NMR (Table 2). Take IPC-1 as an example, the two numbers are 45.7 wt% and 45.74 wt%, respectively. The excellent agreement between the two sets of numbers produced by the vastly different approaches, one nanoscopic and *in situ* whereas the other macroscopic and *ex situ*, further validates the AFM-IR quantitation method. This result also implies that the intermediate phase in these IPCs

https://doi.org/10.1007/s10118-023-3058-4

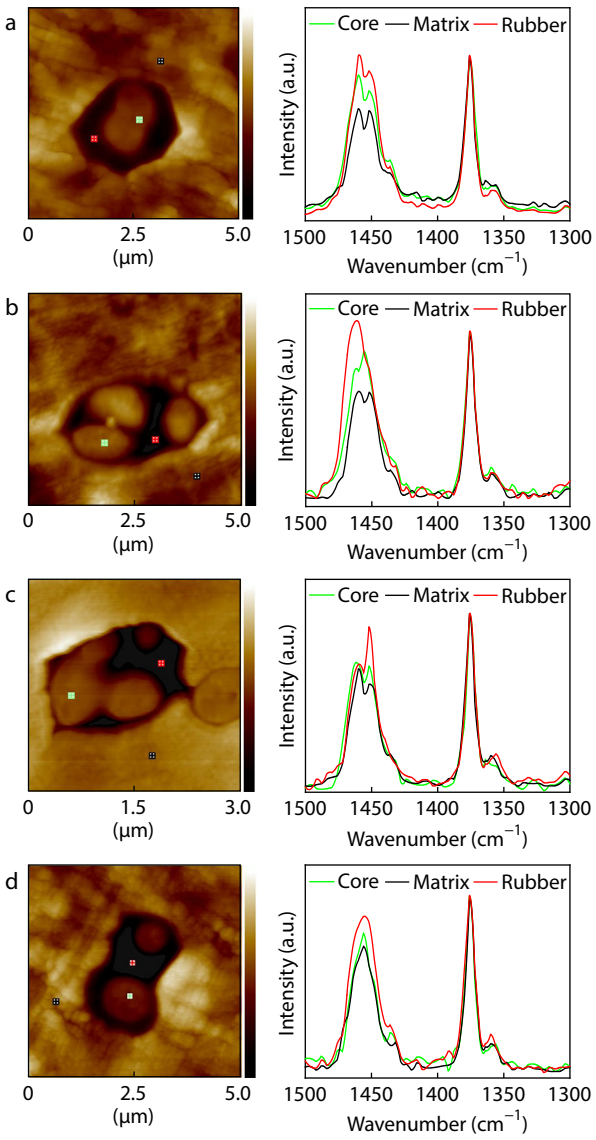

Fig. 5 AFM image of a typical core-shell rubber particle and corresponding AFM-IR spectra acquired at the marked locations in matrix, rubber and core phases, respectively for (a) IPC-1, (b) IPC-2, (c) IPC-3 and (d) IPC-4.

Table 4 Ethylene contents of different phases in IPCs analyzed by AFM-IR (wt%).

Phase	Matrix	Intermediate	Core
IPC-1	0.7±6.5	45.7±8.7	31.0±10.2
IPC-2	0.6±6.2	41.1±10.9	26.8±8.9
IPC-3	−0.2±4.2	34.4±10.5	17.4±5.4
IPC-4	−0.1±5.2	33.0±11.9	19.9±9.3

comprises almost exclusively EPR. On the other hand, the distribution of the block copolymers, EsP and EbP, which is crucial to the formation of the core-shell structure for the rubber particles[3,22] and the mechanical properties of the alloy,[4,38] is more complicated. They can form the core and the outer shell of the dispersed particles.[19,39] However, due to their similarity in chain structure and composition, it is difficult if not impossible to distinguish between EsP and EbP in the particles *in situ*. Recently, we showed that based on the ethylene content in the core phase measured by AFM-IR and the compositions of the EsP and EbP fractions determined by ^{13}C-NMR, the distribution of the two types of block copolymers can be deduced.[29] The rubber particles in the four IPCs are then analyzed using this protocol. For IPC-1, assuming that the core is composed of EsP and EbP, which contains 46.5 wt% and 16.9 wt% ethylene, respectively as determined by ^{13}C-NMR (Table 2), to account for the 31.0 wt% ethylene identified in the core by AFM-IR, the following equation must hold: $46.5X_s + 16.9(1 - X_s) = 31.0$, where X_s is the mass fraction of EsP in the core. This gives an EsP fraction of 0.48 by weight, and EbP fraction of 0.52 accordingly. In other words, the core comprises EsP and EbP in about 1:1 ratio. This ratio matches that of EsP and EbP in IPC-1 determined by fractionation, which yielded contents of 4.15 wt% and 4.04 wt% for the two (Table 2), respectively, with a ratio of ~1:1. Therefore, we conclude that both EsP and EbP compose the core in IPC-1, consistent with the well accepted model.[3,19,23] Using the same method we find that the core phase of IPC-2 also consists of EsP and EbP of a roughly equal amount, with a weight fraction of 0.53 and 0.47, respectively, the ratio of which about the same as that in the alloy (Table 2). The similar distribution of the different copolymer components in the multilayered rubber particles, or in other words the similar multilayer phase structures identified in IPC-1 and IPC-2, is attributed to the similar chain structures between the corresponding copolymer components of the two alloys. In particular, the ethylene sequences in EbP for IPC-1 (n_E=36.4) and IPC-2 (n_E=43.5) are relatively long and therefore able to form PE crystallites, as we observed by DSC (Fig. 2a), contributing to phase separation between EbP fraction and PP matrix phase. The dispersed particle structure is schematically illustrated in Fig. 6(a).

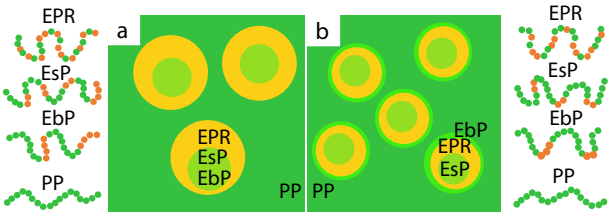

Fig. 6 Schematic illustration of the distribution of different copolymer components in the multilayered rubber particle in (a) IPC-1, IPC-2 and IPC-3, and (b) IPC-4.

In the second group, we reach a same conclusion for IPC-3, that the rigid core consists of both EsP (0.47) and EbP (0.53), which contains 26.7 wt% and 10.0 wt% ethylene, respectively (Table 2), to account for its 17.4 wt% ethylene content found by AFM-IR in the core, and again the weight ratio of the two copolymers in the core phase thus determined matches well that in the entire alloy (5.55 versus 6.23 wt%). However, IPC-4 appears very different. The average ethylene content in the core obtained by AFM-IR is 19.9 wt%, which equals that of EsP fraction in IPC-4 determined by ^{13}C-NMR in conjunction with TREF (19.9 wt%) and much higher than that of EbP (8.6 wt%), indicating that the core must be composed of EsP exclusively. While in Table 2, we notice that there is an appreciable amount of EbP (2.63 wt%, slightly more than that of EsP) in

https://doi.org/10.1007/s10118-023-3058-4

this alloy. Since EbP has been largely excluded from the core, it is logical to conclude that this fraction must have formed the outer shell of the multilayered particle. This outer shell is not observed for IPC-3, and this difference in phase structure between the two IPCs is likely due to the different sequence length and composition of the ethylene-propylene block copolymers.[40] It can be seen in Table 2 that the ethylene units in EbP chains in IPC-3 are present in very long sequences (n_E=112.0), which can readily crystallize into PE crystallites, as revealed by DSC (Fig. 2b), promoting phase separation of the EbP from PP matrix and the rubber phase to form the core phase. In contrast, the EbP chains in IPC-4 comprise short E blocks (n_E=7.5) that do not crystallize and medium P blocks (n_P=51.7), and are expected to have good compatibility with both EPR phase and PP matrix. In other words, the EbP chains prefer to form the interphase layer between the PP matrix and the EPR rubber phase, which can help improve the stability of the particle structure.[23] The combination of the in situ phase composition data by AFM-IR with the chain structure information obtained by TREF and ^{13}C-NMR thus provides evidence in support of the presence of an outer shell in the multilayered rubber particle as described by the widely accepted model.[19] Fig. 6(b) depicts this particle structure schematically. Furthermore, it can be seen from Table 2 that EPRs in IPC-3 and IPC-4 are similar not only in their content in the alloy (12.7 wt% versus 11.0 wt%), but also in chain structure and composition as indicated by the ethylene content and the average E and P segment lengths, yet we see in Table 3 that the rubber particles in IPC-4 (0.31 μm) are much smaller than that in IPC-3 (0.48 μm). This size difference observed can be attributed to the presence of the EbP outer shell in IPC-4, which reduces the interfacial tension between the EPR droplets and the PP matrix, leading to smaller dispersed particles in this alloy.[19,20,23]

By now, we have determined the crystallization, morphology and distribution of the different copolymer fractions for the four IPCs, and are in a position to clarify the effects of the block copolymers on the structure and properties of the alloys. The two alloys in the first group, IPC-1 and IPC-2, are similar in terms of chain structure for each copolymer fraction, which results in similar morphological structure of the two. In particular, their EbP chains comprise long E segments and long P segments, and the former tend to crystallize into PE crystals, driving this fraction to phase separate with the matrix and the rubber and into the core phase; meanwhile the latter promote affinity between EbP and PP matrix, which may be why the cores are often not well separated from the matrix, as can be observed in Figs. 5(a) and 5(b). With similar morphology, IPC-1 exhibits better toughness than IPC-2 and comparable modulus due to its higher EPR content and slightly higher molecular weight. In the second group, while IPC-3 has similar chain characteristics and hence morphological structure as the two alloys in the first group, IPC-4 contains very different EbP chains, with relatively long P blocks but short E segments that are not crystallizable, making them compatible with both the PP matrix and the rubber phase. Therefore, the EbP fraction in IPC-4 tends to form an outer shell for the rubber particles, which reduces the interfacial tension between the rubber and the PP matrix, leading to smaller dispersed particles and more effective toughening of the PP matrix.[23] As a result of this superior morphological structure, IPC-4 achieves better toughness than IPC-3 with a lower rubber content, which in turn benefits the stiffness of the alloy at the same time, killing two birds with one stone.

CONCLUSIONS

For IPC, the microscopic chain structure and composition are the material basis for forming its multilevel phase structure, which in turn governs the mechanical properties of the complex alloy. Quantitation of the phase compositions *in situ* by AFM-IR in conjunction with the chain structure and composition information obtained *ex situ* by TREF and NMR has enabled identification of the distribution of the copolymer fractions in the different phases. By using this approach, we have investigated four IPCs in order to reveal the crucial effects of the structure of EbP on the morphology and properties of the alloy. IPC-1 and IPC-2 are similar in chain structure for each copolymer component, which leads to similar morphological structure. More specifically, the EbP chains contain long E blocks that readily crystallize, which drives the copolymer to phase separate with the rubber phase and the PP matrix, forming the core phase with the EsP. With this similar morphology, a higher EPR content in IPC-1 and slightly higher molecular weight results in its better toughness than IPC-2 and comparable modulus. On the other hand, IPC-3 and IPC-4 are vastly different in EbP structure and alike otherwise. While IPC-3 has similar chain characteristics and hence morphological structure as the previous two, EbP chains in IPC-4 comprise relatively long P blocks but short E segments that are not crystallizable, making the fraction compatible with both the PP matrix and the rubber phase. Consequently, EbP in IPC-4 forms an outer shell for the rubber particles, which reduces the interfacial tension between the rubber and the PP matrix, leading to smaller dispersed particles. This superior morphological structure enables toughening PP with less EPR to achieve both better toughness and a higher modulus at the same time. The findings clarify the critical role EbP plays in IPC, and provide guidance for the design and production of this commercially important material with better properties.

Conflict of Interests

The authors declare no interest conflict.

ACKNOWLEDGMENTS

This work was financially supported by the National Natural Science Foundation of China (No. 52073277) and the Science and Technology Department of Fujian Province (No. 2020HZ06019).

REFERENCES

1 Cecchin, G.; Marchetti, E.; Baruzzi, G. On the mechanism of polypropene growth over $MgCl_2/TiCl_4$ catalyst systems. *Macromol. Chem. Phys.* **2001**, *202*, 1987–1994.
2 Galli, P.; Vecellio, G. Polyolefins: the most promising large-volume

materials for the 21st century. *J. Polym. Sci., Part A: Polym. Chem.* **2004**, *42*, 396–415.
3 Tong, C. Y.; Lan, Y.; Chen, Y.; Chen, Y.; Yang, D. C.; Yang, X. N. The functions of crystallizable ethylene-propylene copolymers in the formation of multiple phase morphology of high impact polypropylene. *J. Appl. Polym. Sci.* **2012**, *123*, 1302–1309.
4 Tan, H. S.; Li, L.; Chen, Z. N.; Song, Y. H.; Zheng, Q. Phase morphology and impact toughness of impact polypropylene copolymer. *Polymer* **2005**, *46*, 3522–3527.
5 Xu, J. T.; Feng, L. X.; Yang, S. L.; Wu, Y. N.; Yang, Y. Q.; Kong, X. M. Separation and identification of ethylene-propylene block copolymer. *Polymer* **1997**, *38*, 4381–4385.
6 Gahleitner, M.; Tranninger, C.; Doshev, P. Heterophasic copolymers of polypropylene: development, design principles, and future challenges. *J. Appl. Polym. Sci.* **2013**, *130*, 3028–3037.
7 Chen, F.; Qiu, B.; Shangguan, Y.; Song, Y.; Zheng, Q. Correlation between impact properties and phase structure in impact polypropylene copolymer. *Mater. Design* **2015**, *69*, 56–63.
8 Kim, G. M.; Michler, G. H. Micromechanical deformation processes in toughened and particle-filled semicrystalline polymers: Part 1. Characterization of deformation processes in dependence on phase morphology. *Polymer* **1998**, *39*, 5689–5697.
9 Liu, X.; Guo, M.; Wei, W. Stress-whitening of high-impact poly(propylene): characterization and analysis. *Macromol. Symp.* **2012**, *312*, 130–138.
10 Li, F.; Gao, Y.; Zhang, Y.; Jiang, W. Design of high impact thermal plastic polymer composites with balanced toughness and rigidity: Toughening with core-shell rubber modifier. *Polymer* **2020**, *191*, 122237.
11 Chen, F.; Shangguan, Y.; Jiang, Y.; Qiu, B.; Luo, G.; Zheng, Q. Toughening with little rigidity loss and mechanism for modified polypropylene by polymer particles with core-shell structure. *Polymer* **2015**, *65*, 81–92.
12 Li, R.; Zhang, X.; Zhao, Y.; Hu, X.; Zhao, X.; Wang, D. New polypropylene blends toughened by polypropylene/poly(ethylene-*co*-propylene) in-reactor alloy: Compositional and morphological influence on mechanical properties. *Polymer* **2009**, *50*, 5124–5133.
13 Cai, H. J.; Luo, X. L.; Ma, D. Z.; Wang, J. M.; Tan, H. S. Structure and properties of impact copolymer polypropylene. I. Chain structure. *J. Appl. Polym. Sci.* **1999**, *71*, 93–101.
14 Cheruthazhekatt, S.; Pijpers, T. F. J.; Harding, G. W.; Mathot, V. B. F.; Pasch, H. Multidimensional analysis of the complex composition of impact polypropylene copolymers: combination of TREF, SEC-FTIR-HPer DSC, and high temperature 2D-LC. *Macromolecules* **2012**, *45*, 2025–2034.
15 Fernandez, A.; Teresa Exposito, M.; Pena, B.; Berger, R.; Shu, J.; Graf, R.; Spiess, H. W.; Garcia-Munoz, R. A. Molecular structure and local dynamic in impact polypropylene copolymers studied by preparative TREF, solid state NMR spectroscopy, and SFM microscopy. *Polymer* **2015**, *61*, 87–98.
16 Xue, Y.; Fan, Y.; Bo, S.; Ji, X. Characterization of the microstructure of impact polypropylene alloys by preparative temperature rising elution fractionation. *Eur. Polym. J.* **2011**, *47*, 1646–1653.
17 Zhang, Y. Q.; Fan, Z. Q.; Feng, L. X. Influences of copolymerization conditions on the structure and properties of isotactic polypropylene/ethylene-propylene random copolymerin situ blends. *J. Appl. Polym. Sci.* **2002**, *84*, 445–453.
18 Zhu, H.; Han, C. C.; Wang, D. Phase structure and crystallization behavior of polypropylene in-reactor alloys: insights from both inter- and intramolecular compositional heterogeneity. *Macromolecules* **2008**, *41*, 826–833.
19 Zhang, C.; Shangguan, Y.; Chen, R.; Wu, Y.; Chen, F.; Zheng, Q.; Hu, G. Morphology, microstructure and compatibility of impact polypropylene copolymer. *Polymer* **2010**, *51*, 4969–4977.
20 Chen, Y.; Chen, Y.; Chen, W.; Yang, D. Multilayered core–shell structure of the dispersed phase in high-impact polypropylene. *J. Appl. Polym. Sci.* **2008**, *108*, 2379–2385.
21 Song, S.; Feng, J.; Wu, P. Relaxation of shear-enhanced crystallization in impact-resistant polypropylene copolymer: insight from morphological evolution upon thermal treatment. *Polymer* **2010**, *51*, 5267–5275.
22 Qiu, B. W.; Chen, F.; Shangguan, Y. G.; Lin, Y.; Zheng, Q. Effects of composition on microstructure and crystallization behavior for impact polypropylene copolymer investigated by restructuring the complex core-shell dispersed particles in ternary blends. *Chinese J. Polym. Sci.* **2015**, *33*, 95–108.
23 Rungswang, W.; Saendee, P.; Thitisuk, B.; Pathaweeisariyakul, T.; Cheevasrirungruang, W. Role of crystalline ethylene-propylene copolymer on mechanical properties of impact polypropylene copolymer. *J. Appl. Polym. Sci.* **2013**, *128*, 3131–3140.
24 Dazzi, A.; Glotin, F.; Carminati, R. Theory of infrared nanospectroscopy by photothermal induced resonance. *J. Appl. Phys.* **2010**, *107*, 124519.
25 Dazzi, A.; Prater, C. B. AFM-IR: technology and applications in nanoscale infrared spectroscopy and chemical imaging. *Chem. Rev.* **2017**, *117*, 5146–5173.
26 Dazzi, A.; Prazeres, R.; Glotin, F.; Ortega, J. M. Local infrared microspectroscopy with subwavelength spatial resolution with an atomic force microscope tip used as a photothermal sensor. *Opt. Lett.* **2005**, *30*, 2388–2390.
27 Tang, F.; Bao, P.; Su, Z. Analysis of nanodomain composition in high-impact polypropylene by atomic force microscopy-infrared. *Anal. Chem.* **2016**, *88*, 4926–4930.
28 Tang, F.; Bao, P.; Roy, A.; Wang, Y.; Su, Z. *In-situ* spectroscopic and thermal analyses of phase domains in high-impact polypropylene. *Polymer* **2018**, *142*, 155–163.
29 Li, C.; Wang, Z.; Liu, W.; Ji, X.; Su, Z. Copolymer distribution in core-shell rubber particles in high-impact polypropylene investigated by atomic force microscopy-infrared. *Macromolecules* **2020**, *53*, 2686–2693.
30 Agosti, E.; Zerbi, G.; Ward, I. M. Structure of the skin and core of ultradrawn polyethylene films by vibrational spectroscopy. *Polymer* **1992**, *33*, 4219–4229.
31 Kissin, Y. V.; Tsvetkova, V. I.; Chirkov, N. M. The stereoregularity of polypropylene from IR and NMR data. *Eur. Polym. J.* **1972**, *8*, 529–546.
32 Hagemann, H.; Snyder, R. G.; Peacock, A. J.; Mandelkern, L. Quantitative infrared methods for the measurement of crystallinity and its temperature dependence: polyethylene. *Macromolecules* **2002**, *22*, 3600–3606.
33 Zhu, X.; Yan, D.; Yao, H.; Zhu, P. *In situ* FTIR spectroscopic study of the regularity bands and partial-order melts of isotactic poly(propylene). *Macromol. Rapid Commun*. **2000,** *21*, 354-357.
34 Chen, J. H.; Zhong, J. C.; Cai, Y. H.; Su, W. B.; Yang, Y. B. Morphology and thermal properties in the binary blends of poly(propylene-*co*-ethylene) copolymer and isotactic polypropylene with polyethylene. *Polymer* **2007**, *48*, 2946–2957.
35 Li, R.; Ji, X. L. The relationship between ethylene content and properties of high impact polypropylene. *Manuscript in preparation*.
36 Liu, W.; Zhang, J.; Hong, M.; Li, P.; Xue, Y.; Chen, Q.; Ji, X. Chain microstructure of two highly impact polypropylene resins with good balance between stiffness and toughness. *Polymer* **2020**,

https://doi.org/10.1007/s10118-023-3058-4

188, 122146.
37 van der Wal, A.; Verheul, A. J. J.; Gaymans, R. J. Polypropylene–rubber blends: 4. The effect of the rubber particle size on the fracture behaviour at low and high test speed. *Polymer* **1999**, *40*, 6057–6065.
38 Kim, S. D.; Choi, Y.; Choi, W.; Choi, C.; Chun, Y. S. Effect of ethylene-propylene copolymer composition on morphology and surface properties of impact poly(propylene) copolymer. *Macromol. Symp.* **2012**, *312*, 27–33.
39 Rungswang, W.; Jarumaneeroj, C.; Jirasukho, P.; Juabrum, S.; Pakawanit, P.; Soontaranon, S.; Rugmai, S. Time-resolved SAXS/WAXD under tensile deformation: role of segmental ethylene-propylene copolymers in impact-resistant polypropylene copolymers. *ACS Appl. Polym. Mater.* **2021**, *3*, 6394–6406.
40 Santonja-Blasco, L.; Rungswang, W.; Alamo, R. G. Influence of chain microstructure on liquid-liquid phase structure and crystallization of dual reactor Ziegler-Natta made impact propylene–ethylene copolymers. *Ind. Eng. Chem. Res.* **2017**, *56*, 3270–3282.

https://doi.org/10.1007/s10118-023-3058-4